International Journal of Coal Geology 121 (2014) 19–25

Contents lists available at ScienceDirect

International Journal of Coal Geology

journal homepage: www.elsevier.com/locate/ijcoalgeo

# The relationship between micro-Raman spectral parameters and reflectance of solid bitumen

Qin Zhou [a,b], Xianming Xiao [a,*], Lei Pan [a,b], Hui Tian [a]

[a] State Key Laboratory of Organic Geochemistry, Guangzhou Institute of Geochemistry, Chinese Academy of Sciences, Guangzhou 510640, China
[b] Graduate University of the Chinese Academy of Sciences, Beijing 100049, China

ARTICLE INFO

*Article history:*
Received 18 September 2013
Received in revised form 25 October 2013
Accepted 29 October 2013
Available online 6 November 2013

*Keywords:*
Solid bitumen
Raman spectral parameter
Bitumen reflectance
Maturity indicator

ABSTRACT

Solid bitumen occurs widely in the Early Paleozoic and Precambrian strata and its reflectance is a generally-accepted indicator for thermal maturity. Even though some recent papers have been published concerning the Raman characteristics and spectral parameters of solid bitumen, a systematic investigation on the relationship between the Raman spectral parameters and thermal maturity of solid bitumen is still lacking. In this study, a low maturity solid bitumen sample was pyrolysed under laboratory-controlled conditions to obtain a suite of artificial bitumen samples with different maturities (BRo = 1.1–4.81%), which are used to investigate the relationships between Raman spectral parameters and reflectance of solid bitumen. The Raman spectral parameters of the artificial bitumens, including band position ($W_D$ and $W_G$), band separation (RBS), full width at half maximum (FWHM-D and FWHM-G), and band intensity ratio ($I_D/I_G$) are all related to the bitumen reflectance, but with considerably different correlations, constrained apparently by thermal maturity. Linear regressions were performed between these parameters and bitumen reflectance, and two parameters with higher correlation were selected. They are RBS (within 1.5–3.5% of BRo) and $I_D/I_G$ (within 3.0–5.0% of BRo), with a correlation coefficient as high as 0.97. It is believed that the two Raman spectral parameters of solid bitumen will be of significant practical use for the maturity assessment of the Early Paleozoic and Precambrian strata when standard measurement and curve fitting procedures are utilized.



## 1. Introduction

In recent decades, numerous papers have reported that the Raman spectral characteristics and related parameters of geological solid organic matter, including coals, carboniferous fossils and carbonaceous materials, can be used as indicators for thermal maturity (i.e., Beyssac et al., 2002; Ferrari and Robertson, 2000; Guedes et al., 2010; Kelemen and Fang, 2001; Kwiecinska et al., 2010; Muirhead et al., 2012; Quirico et al., 2005, 2009; Rahl et al., 2005; Roberts et al., 1995; Schopf et al., 2005; Schopf and Kudryavtsev, 2009; Zeng and Wu, 2007). Detailed studies have focused on coals with different rank (Green et al., 1983; Guedes et al., 2010; Kelemen and Fang, 2001; Marques et al., 2009; Quirico et al., 2005; Sonibare et al., 2010). The first-order characteristic bands of the Raman spectrum of carbon in coals have been found to generally occur at approximately 1350 $cm^{-1}$ (D band) and 1580 $cm^{-1}$ (G band) (Guedes et al., 2010; Kwiecinska et al., 2010; Wopenka and Pasteris, 1993). The D band is also called D1 band (Marques et al., 2009; Wopenka and Pasteris, 1993) or A band (Kelemen and Fang, 2001), and it originates in vibrations of the disordered structure of carbonaceous material (Beyssac et al., 2002, 2003). The G band is assigned to vibrations of the ordered (graphitic) structure (Beyssac et al., 2002, 2003). With increasing thermal maturity, these two bands show regular changes in their position, FWHM (full width at half maximum) and intensity, which have been shown to be clearly correlated with maturity (Guedes et al., 2010; Kelemen and Fang, 2001; Kostova et al., 2012; Quirico et al., 2005).

Solid bitumen is a type of organic matter extensively occurring in petroleum-bearing basins and also in Precambrian shale-rich strata (Jacob, 1989; Lomando, 1992; Schoenherr et al., 2007). Available data indicate that despite the fact that solid bitumen is different from coal in their precursors, their Raman spectral characteristics and related changes in the process of thermal maturation are very similar (Court et al., 2007; Jehlicka et al., 2003). However, as yet few studies have been focused on the Raman spectral characteristics of solid bitumen, a systematic study is lacking on changes to the Raman spectral parameters in the process of thermal maturation. In the present study, a solid bitumen sample with a low maturity was pyrolysed to obtain a suite of artificial bitumen samples with different maturities, then their Raman spectra were investigated, and the changes of the parameters with the maturity were revealed. Combined with data from natural samples, the use of Raman spectral parameters of natural and synthetic bitumen as maturity indicators was explored.

* Corresponding author. Tel.: +86 20 85290176.
*E-mail address:* xmxiao@gig.ac.cn (X. Xiao).

0166-5162/$ – see front matter © 2013 Elsevier B.V. All rights reserved.
http://dx.doi.org/10.1016/j.coal.2013.10.013

## 2. Sample and experiment

The original solid bitumen sample was collected from a bitumen vein in the Permian strata of the Changjianggou area, western Sichuan Basin of southwestern China. As the outcrop resulted from the cutting of a new road, the sample is fresh and has not been or very little subjected to weathering and oxidation. The bitumen is of low maturity, with a bitumen reflectance (BRo) of 0.43%. Since the Permian organic rich mudstone in this area is in a lower mature stage, it is believed that the bitumen was derived from the Early Paleozoic marine shales, which are widely distributed over the whole Sichuan Basin (Zhou et al., 2013). The bitumen was powdered to 80-mesh, and heated in a vacuumed autoclave to 350 °C, 400 °C, 450 °C, 500 °C, 550 °C, 600 °C, 650 °C, 700 °C and 750 °C, respectively, remaining for 24 h at each preset temperature point. In this way artificial bitumen samples with different maturities were obtained. These samples were prepared as polished blocks for bitumen reflectance measurements and Raman spectral analyses.

Bitumen reflectance was measured using a 3Y-Leica DMR XP microphotometer, according to the usual method of coal petrology as described by Dai et al. (2012). Depending on the maturity of the bitumen sample to be measured, a matching standard sample was selected for use from the three available standard samples of YAG-08-57 ($R_o$ = 0.904%), NR1149 ($R_o$ = 1.24%) and cubic zirconia ($R_o$ = 3.11%). An oil immersion objective 50/0.85 was used. For each sample, 50 individual bitumen particles were measured and their mean value was taken as the bitumen reflectance.

A HORIBA-JY LabRAM spectrometer equipped with a He–Ne laser (source power 30 mV) was applied for Raman spectral analysis of the

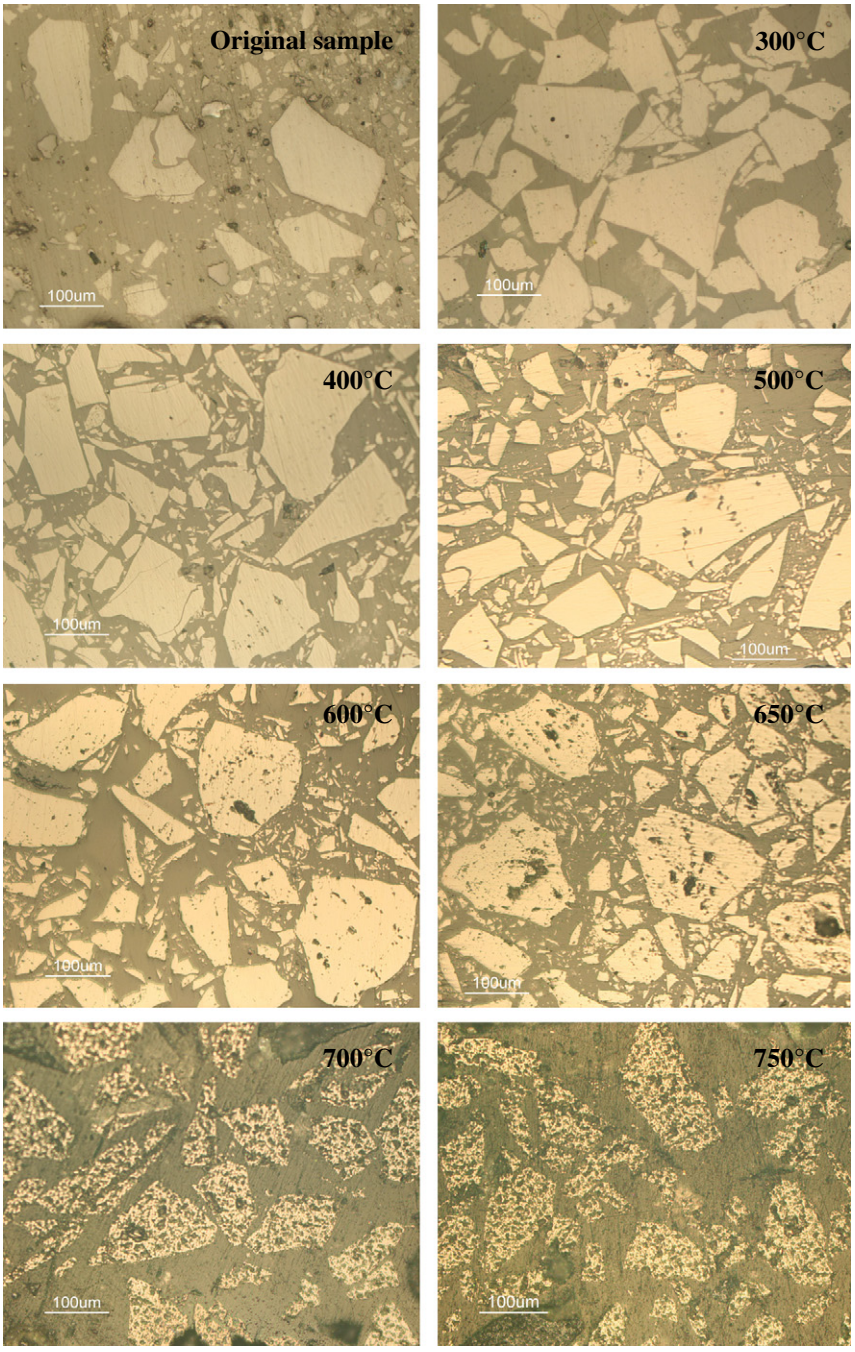


**Fig. 1.** The solid bitumen at different heated temperatures. Reflect light and oil immersion of optical microscope.

bitumen samples. Raman spectra were obtained with a density filter to avoid thermal decomposition of the samples. The main measuring conditions are: laser wavelength 532 nm, exposure time 10–20 s, and scanning wave number range 1000–3000 $cm^{-1}$. For each sample five individual bitumen particles were measured. Curve fitting for the determination of spectral parameters was performed with the GaussLorentz model in the instrument software, and all the analytical and calculation procedures were conducted following Beyssac et al. (2003).

## 3. Results and discussion

### 3.1. Optical characteristics of bitumen

Fig. 1 shows some photomicrographs of the solid bitumen at different pyrolytic temperatures. For the unheated sample, the bitumen particles exhibit homogeneous optical properties, smooth surfaces, and no voids. When the temperature is increased to 500 °C, the bitumen particles still show smooth polished surfaces with few voids but an obvious increase in the reflectance. By 600 °C, some voids occur in the bitumen particles, however, the polished surfaces are still smooth. Over 650 °C, voids rapidly increase, and up to 700 °C, the polished surfaces of the bitumen particles are filled with voids and show a structure similar to that of coke.

In the process of the pyrolysis, the reflectance of the bitumen continues to increase. To quantify the change of bitumen reflectance, an aperture diaphragm size had to be adjusted depending upon the optic properties of the bitumen. For the bitumen heated to a temperature below 650 °C, a standard aperture diaphragm with a diameter of 10 μm was used to measure the reflectance. For the bitumen heated at 700 °C and 750 °C showing void development at its polished surfaces, an aperture diaphragm as small as 2–5 μm had to be used and a relatively smooth surface with few apparent voids was targeted for the reflectance measurement. Fig. 2 shows the relationship between the pyrolytic temperature of the bitumen and its average reflectance, the two variables being linearly correlated with a correlation coefficient as high as 0.99. Consequently, the average bitumen reflectance can be used to represent the thermal maturity, standing for the pyrolytic temperature of the bitumen.

### 3.2. Raman spectral characteristics and parameters of bitumen

Raman spectra of the bitumen at different heated temperatures are illustrated in Fig. 3. Similar to coals, the Raman spectra of these samples generally show two first-order characteristic bands, i.e., the D band at 1320–1330 $cm^{-1}$ and G band at 1590–1650 $cm^{-1}$. Even the unheated sample presents these two characteristic bands. With temperature increasing, both D and G bands tend to exhibit an increasing intensity, and this is particularly for D band. When samples were heated to temperatures below 600 °C, the D band has a distinctly weaker intensity than the G band. When samples were heated to a temperature over 600 °C, the D band shows an apparent increase in intensity, and at 750 °C its intensity can be comparable to that of the G band. In addition, the two band positions vary in a regular trend with temperature increasing. The D band firstly shifts to lower frequencies, and then to higher frequencies, with a turning point at around 600 °C. By contrast, the G band shows only smaller changes in position, shifting to higher frequencies with increasing maturity (Fig. 3). Similar trends in band positions were also observed for coals and kerogens (Guedes et al., 2010, 2012; Kelemen and Fang, 2001; Marques et al., 2009; Sonibare et al., 2010) and also for bitumens (Jehlicka et al., 2003) subjected to different degrees of thermal maturation.

By comparison with the Raman spectral parameters for coals (Kelemen and Fang, 2001; Kostova et al., 2012; Quirico et al., 2005; Sonibare et al., 2010), the shape, relative intensity ratio, and position changes for the D and G bands in the process of thermal maturation can be quantitatively represented using the following parameters:

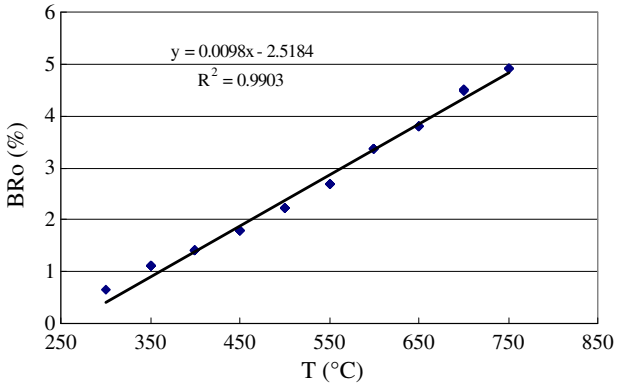


**Fig. 2.** Relationship between reflectance (BRo%) and its pyrolytic temperature of the bitumen sample.

(1) Band position: $W_D$ and $W_G$
(2) Band separation: RBS = $W_G$–$W_D$
(3) Full width at half maximum: FWHM-D and FWHM-G
(4) Band intensity ratio: $I_D/I_G$
(5) Band area ratio: $A_D/A_G$.

These data plus bitumen reflectance (BRo) values are shown in Table 1 and the relationships between these parameters and bitumen reflectance are illustrated in Fig. 4. These parameters, to some extent, are all correlated with bitumen reflectance. In different patterns, the same parameter is distinctively correlated with BRo at different stages of maturation. With maturity increasing, $W_G$ is slightly increased from 1595 to 1600 $cm^{-1}$ when BRo <2.0%, but becomes generally stabilized at ca. 1600 $cm^{-1}$ after BRo >2.0%. $W_D$ varies randomly between 1360 and 1370 $cm^{-1}$ when BRo <2.0%, but shifts apparently toward lower frequencies from 1360 $cm^{-1}$ to 1325 $cm^{-1}$ when BRo ranges from 2.0 to 3.5%. When BRo >3.5%, $W_D$ tends to increase slightly. Constrained by $W_D$ and $W_G$ changes, BRS increases with maturity increasing before BRo <3.5%, but tends to decrease slightly with further maturity increasing. With maturity increasing, both FWHM-D and FWHM-G tend to decrease. FWHM-D changes inconspicuously when BRo <1.5%, but decreases markedly from 250 $cm^{-1}$ to 120 $cm^{-1}$ after BRo >1.5%. FWHM-G decreases significantly from 120 $cm^{-1}$ to 55 $cm^{-1}$ when BRo <2.5%, but becomes stable at ca. 55 $cm^{-1}$ when BRo >2.5%. With maturity increasing, $I_D/I_G$ decreases slightly with scattered results when BRo <3.0%. However, this parameter increases rapidly and tends

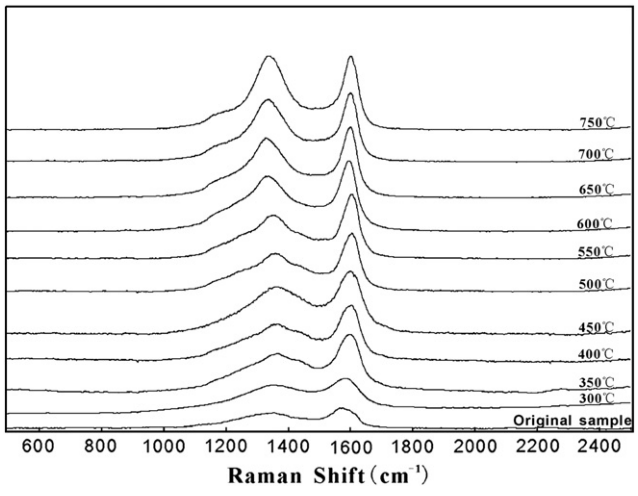


**Fig. 3.** Typical Raman spectra of the bitumen at different heated temperatures.

to be linearly correlated with BRo when BRo >3.0%. Changes of $A_D/A_G$ and FWHM-D/FWHM-G are similar with increasing maturity. The two parameters first increase, then decrease significantly, with turning points at BRo 3.0% and 2.5%, respectively.

### 3.3. Maturity indicators derived from Raman spectra

Based on the above observations, it is clear that the Raman spectral parameters of a solid bitumen can reflect its maturity. Parameters including $W_D$, RBS, FWHM-D, $I_D/I_G$, and FWDH-D/FWDH-G can be recommended, even though they are well correlated with bitumen reflectance over only certain ranges of maturity defined as follows: $W_D$ within the BRo range of 1.5–3.5%, RBS within BRo 1.5–3.5%, FWHM-D within BRo 1.5–5.0%, and $I_D/I_G$ and FWDH-D/FWDH-G with BRo >3.0%. Linear regressions of the relationships of these parameters with BRo for their best-applied maturation ranges (Fig. 5) are as follows:

$$\mathrm{BRo} = 85.31 - 0.0613 \times W_D \left(R^2 = 0.93\right)$$
$$\mathrm{BRo} = 0.0626 \times \mathrm{RBS} - 13.17 \left(R^2 = 0.97\right)$$
$$\mathrm{BRo} = 7.96 - 0.0245 \times \mathrm{FWDH-D} \left(R^2 = 0.90\right)$$
$$\mathrm{BRo} = 5.64 \times I_D/I_G - 0.745 \left(R^2 = 0.97\right)$$
$$\mathrm{BRo} = 7.17 - 1.065 \times \mathrm{FWDH-D/FWDH-G} \left(R^2 = 0.94\right).$$

It can be seen that BRo is best correlated with RBS and $I_D/I_G$. In both cases, the correlation coefficients are as high as 0.97.

**Table 1**
Reflectance values and Raman spectral parameters of the studied bitumen sample at different heated temperatures.

| Temperature (°C)-measured point | BRo (%) | $W_D$ ($cm^{-1}$) | $W_G$ ($cm^{-1}$) | RBS ($cm^{-1}$) | FWHM-D ($cm^{-1}$) | FWHM-G ($cm^{-1}$) | $I_D/I_G$ | $A_D/A_G$ |
|---|---|---|---|---|---|---|---|---|
| Original | 0.43 | 1363.00 | 1595.04 | 231.71 | 261.64 | 110.40 | 0.76 | 2.37 |
| 300-1 | 0.65 | 1362.39 | 1594.92 | 232.53 | 262.95 | 110.64 | 0.76 | 2.38 |
| 300-2 | | 1359.06 | 1591.6 | 232.54 | 278.57 | 117.15 | 0.78 | 2.38 |
| 300-3 | | 1359.06 | 1598.28 | 239.22 | 265.55 | 115.85 | 0.74 | 2.29 |
| 300-4 | | 1365.71 | 1595.6 | 229.89 | 275.96 | 109.34 | 0.67 | 2.53 |
| 300-5 | | 1368.36 | 1597.66 | 229.3 | 256.44 | 101.94 | 0.77 | 2.52 |
| 350-1 | 1.15 | 1364.72 | 1598.94 | 234.22 | 279.87 | 89.40 | 0.68 | 3.132 |
| 350-2 | | 1366.70 | 1600.18 | 233.48 | 277.27 | 80.70 | 0.67 | 3.434 |
| 350-3 | | 1365.80 | 1599.89 | 234.09 | 303.30 | 85.70 | 0.67 | 3.54 |
| 350-4 | | 1365.67 | 1601.53 | 235.86 | 270.76 | 75.50 | 0.75 | 3.59 |
| 350-5 | | 1366.86 | 1601.53 | 234.07 | 274.66 | 78.10 | 0.73 | 3.52 |
| 400-1 | 1.40 | 1365.38 | 1601.98 | 236.6 | 256.44 | 68.99 | 0.63 | 3.72 |
| 400-2 | | 1364.52 | 1601.05 | 236.53 | 264.25 | 70.29 | 0.75 | 3.76 |
| 400-3 | | 1364.45 | 1601.58 | 237.13 | 279.87 | 71.59 | 0.68 | 3.91 |
| 400-4 | | 1367.02 | 1603.62 | 236.6 | 268.15 | 65.08 | 0.66 | 4.12 |
| 400-5 | | 1363.41 | 1599.74 | 236.33 | 274.66 | 74.19 | 0.65 | 3.70 |
| 450-1 | 1.79 | 1361.83 | 1600.39 | 238.56 | 242.12 | 70.81 | 0.69 | 3.42 |
| 450-2 | | 1360.63 | 1600.69 | 240.06 | 235.61 | 67.21 | 0.73 | 3.51 |
| 450-3 | | 1356.17 | 1596.09 | 239.92 | 229.11 | 73.73 | 0.728 | 3.11 |
| 450-4 | | 1365.94 | 1596.35 | 238.74 | 221.30 | 77.63 | 0.68 | 2.85 |
| 450-5 | | 1359.43 | 1598.3 | 238.19 | 229.11 | 63.42 | 0.76 | 3.61 |
| 500-1 | 2.23 | 1355.71 | 1602.8 | 247.09 | 247.33 | 61.18 | 0.66 | 4.04 |
| 500-2 | | 1359.03 | 1603.56 | 244.53 | 247.33 | 59.88 | 0.65 | 4.13 |
| 500-3 | | 1358.78 | 1604.27 | 245.49 | 247.33 | 59.88 | 0.66 | 4.13 |
| 500-4 | | 1358.78 | 1603.68 | 244.9 | 246.03 | 61.18 | 0.72 | 4.02 |
| 500-5 | | 1355.71 | 1601.53 | 245.82 | 230.64 | 70.29 | 0.68 | 3.28 |
| 550-1 | 2.69 | 1351.77 | 1605.03 | 253.26 | 209.58 | 52.07 | 0.71 | 4.03 |
| 550-2 | | 1348.61 | 1603.88 | 255.27 | 231.71 | 53.37 | 0.71 | 4.34 |
| 550-3 | | 1349.06 | 1602.42 | 253.28 | 225.20 | 53.37 | 0.70 | 4.22 |
| 550-4 | | 1349.06 | 1602.00 | 252.94 | 214.79 | 58.57 | 0.68 | 3.67 |
| 550-5 | | 1350.46 | 1602.77 | 252.31 | 226.50 | 53.37 | 0.69 | 4.24 |
| 600-1 | 3.36 | 1333.65 | 1599.05 | 265.4 | 223.80 | 61.18 | 0.71 | 3.66 |
| 600-2 | | 1333.27 | 1599.92 | 266.65 | 217.39 | 57.27 | 0.73 | 3.80 |
| 600-3 | | 1330.69 | 1598.36 | 267.67 | 212.18 | 55.97 | 0.73 | 3.79 |
| 600-4 | | 1331.08 | 1601.00 | 269.92 | 205.67 | 55.97 | 0.73 | 3.67 |
| 600-5 | | 1334.37 | 1599.13 | 264.76 | 212.18 | 61.18 | 0.74 | 3.47 |
| 650-1 | 3.80 | 1334.05 | 1602.52 | 268.47 | 160.11 | 52.07 | 0.80 | 3.08 |
| 650-2 | | 1331.44 | 1601.30 | 269.86 | 160.11 | 53.37 | 0.81 | 3.00 |
| 650-3 | | 1327.54 | 1600.25 | 272.71 | 149.70 | 50.77 | 0.81 | 2.951 |
| 650-4 | | 1333.39 | 1600.65 | 267.26 | 165.32 | 54.67 | 0.81 | 3.02 |
| 650-5 | | 1333.39 | 1601.65 | 268.26 | 165.32 | 54.67 | 0.81 | 3.02 |
| 700-1 | 4.50 | 1328.19 | 1598.95 | 270.76 | 134.08 | 54.67 | 0.90 | 2.45 |
| 700-2 | | 1331.44 | 1599.60 | 268.16 | 137.98 | 55.97 | 0.92 | 2.47 |
| 700-3 | | 1338.6 | 1600.25 | 261.65 | 143.19 | 54.67 | 0.90 | 2.62 |
| 700-4 | | 1334.58 | 1600.25 | 265.67 | 141.89 | 54.67 | 0.90 | 2.60 |
| 700-5 | | 1337.30 | 1599.60 | 262.30 | 140.59 | 54.67 | 0.91 | 2.57 |
| 750-1 | 4.81 | 1341.20 | 1601.55 | 260.35 | 127.57 | 54.67 | 0.99 | 2.33 |
| 750-2 | | 1336.00 | 1602.20 | 266.20 | 122.36 | 54.67 | 1.00 | 2.24 |
| 750-3 | | 1338.60 | 1600.25 | 261.65 | 127.57 | 58.58 | 2.00 | 2.18 |
| 750-4 | | 1339.25 | 1597.65 | 258.40 | 123.67 | 52.48 | 1.01 | 2.36 |
| 750-5 | | 1337.95 | 1604.16 | 266.21 | 123.67 | 59.46 | 1.011 | 2.08 |

Notation: $W_D$ and $W_G$, Band position; BRo: Average bitumen reflectance; RBS = $W_G$–$W_D$, band separation; FWHM-D and FWHM-G, Full width at half maximum; $I_D/I_G$, Band intensity ratio; $A_D/A_G$, Band area ratio.

Previous studies have demonstrated that the Raman spectral characteristics of artificial samples are comparable to those of natural samples (Kelemen and Fang, 2001). In order to assess the possible geological application of the correlation relationships established above, data from some natural bitumen samples were included in the correlation diagrams (Fig. 5) established in this study. The Raman spectral data of the natural samples were drawn from Liu et al. (2013). These samples were collected from some boreholes and bitumen mines from Sichuan Basin

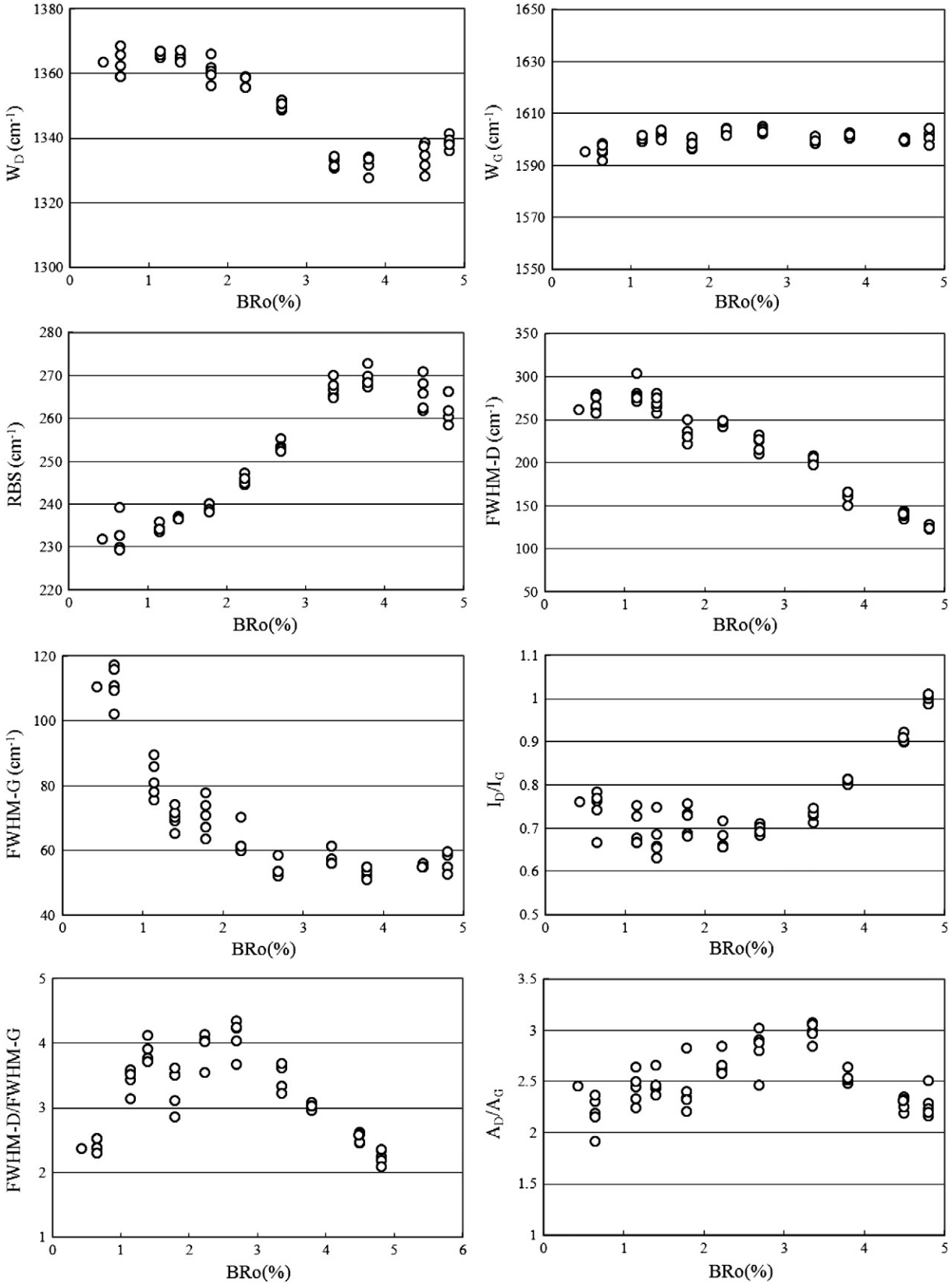


**Fig. 4.** Relations between Raman spectral parameters (see text) and BRo of the artificial bitumen samples.

and other Upper Yangzi region. Their hosted rocks are all Lower Paleozoic carbonate. These bitumens are matured to a high maturity, with BRo values ranging from 1.98% to 4.10%. Regional petroleum geological observations indicate that they were probably derived from oil generated from the Lower Cambrian and/or Lower Silurian marine black shales (i.e. Huang et al., 2011; Lin et al., 2011). Their Raman spectral data were obtained in the same laboratory, using the same instrument, under the same test conditions and curve fitting procedure, as used in the present study, thus the two suites of data should be comparable. As shown in Fig. 5, the data points from the natural bitumen samples are basically consistent with those from the artificial bitumen samples of this study. The data of RBS, $W_D$, $I_D/I_G$, and FWHM-D/FWHM-G are in good agreement, but the FWDH-D data are rather scattered. The natural samples show smaller FWDH-D values than the artificial samples at the same BRo (i.e., the narrower D bands). Whether this characteristic is in particular related to the geological conditions, such as lower temperature and higher pressure, requires further study.

In summary, it can be concluded that among the Raman spectral parameters for solid bitumen, RBS and $I_D/I_G$ are the best maturity indicators, applying respectively to the bitumen with moderate to high maturity (BRo < 3.5%) and to the bitumen with very high maturity (BRo > 3.0%).

### 3.4. Possible application of Raman spectral parameters as maturity indicators

The Early Paleozoic and Precambrian shale-rich strata generally lack vitrinite and fluorescent macerals due to their age and high maturity, therefore conventional maturity indicators (e.g., vitrinite reflectance, fluorescence parameters) cannot be applied to their maturity determination. Solid bitumen occurs widely in these strata (including reservoir rocks and carrier beds; Fu et al., 1989), and in organic-rich shales (Carolyn and Thompson-Rizer, 1987; Xiao et al., 2000), thus bitumen reflectance is the most commonly used maturity indicator (Jacob, 1985, 1989; Rogers et al., 1974). However, bitumen reflectance has some

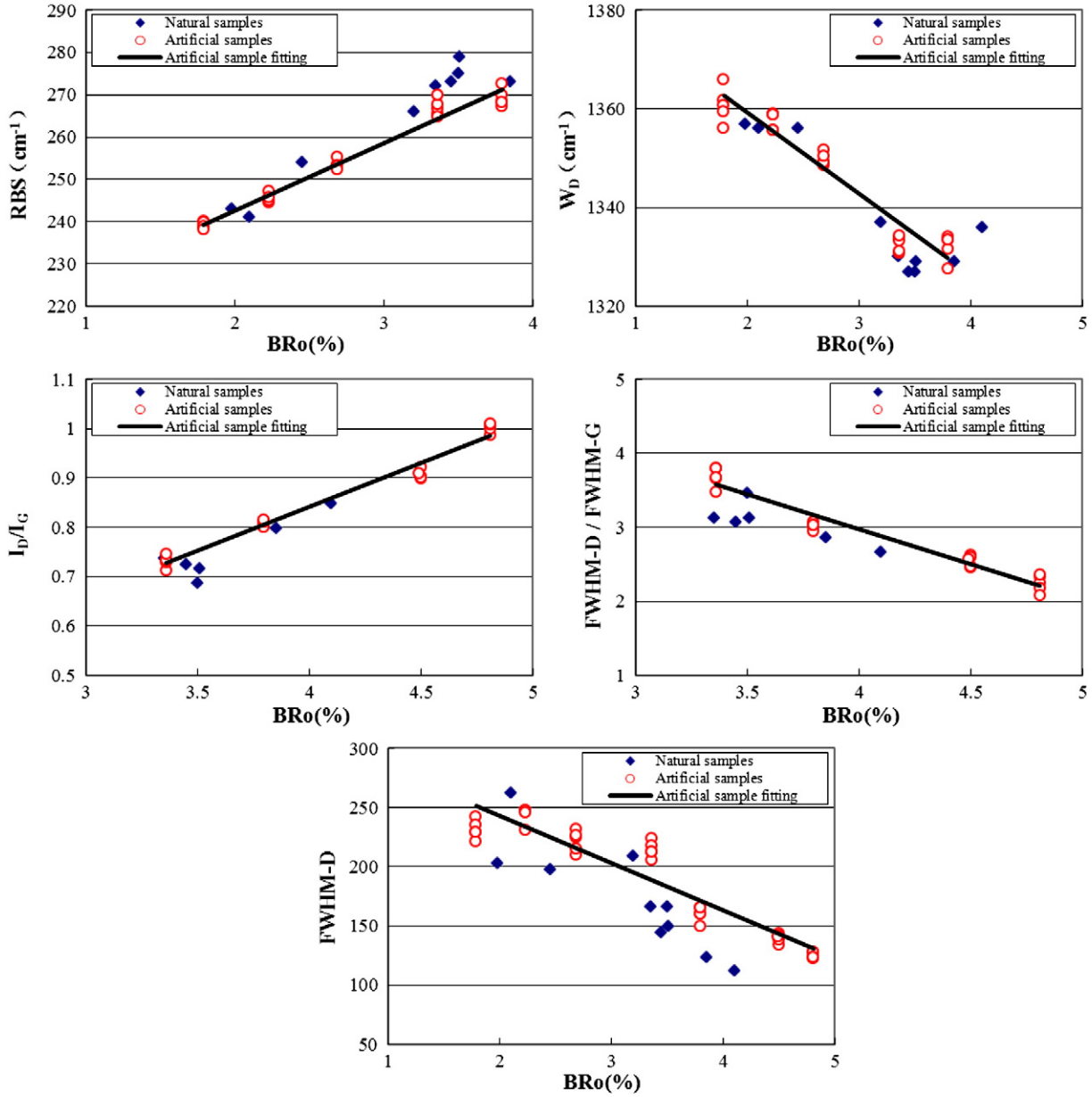


**Fig. 5.** Correlations between the Raman spectral parameters and BRo of the artificial bitumen samples over the selected maturity ranges in comparison with Raman data on natural bitumens. The natural bitumen data are from Liu et al. (2013).

limitations in practical application. For example, bitumen particles are generally very fine in size (<5–10um), and in some cases, show a very strong optical anisotropy, making it very difficult to obtain accurate reflectance measurements (Fu et al., 1989; Xiao et al., 2000). In contrast, Raman spectral parameters of solid bitumen could solve this problem. The advantages of Raman spectral method include: (1) requirement of a small amount of sample (dozens of mg), (2) very fine-grained particles (as small as 1 μm) that could be used (Guedes et al., 2010; Schopf et al., 2005; Schopf and Kudryavtsev, 2009), and (3) less dispersion of the data compared with reflectance; hence, the reliable Raman spectral parameters can be obtained from only a few measured points (Liu et al., 2013).

Previous studies have also discussed the influence of factors except maturity on the Raman spectral parameters of solid organic matter, including their precursors (Quirico et al., 2009), fluids (Guedes et al., 2005), measurement conditions (laser wavelength, excitation time), sample preparation (powder sample or polished thin section sample), and models and procedures for curve fitting (Beyssac et al., 2003; Quirico et al., 2005). These factors affect the magnitude of Raman spectral parameters of solid organic matter, accounting for poor agreement among results from different authors. Experience in establishing the international standard method for vitrinite reflectance measurement should be applied to the Raman spectral measurements and parameter determination through curve-fitting procedures for solid bitumens. In this way, the general application of the Raman spectral parameters as maturity indicators would become possible.

## 4. Conclusions

The following major conclusions of the present study are:

(1) The two first-order bands, i.e., the D and G bands of the Raman spectrum of carbon from a suite of artificially-matured bitumen samples show regular changes in their intensity, shape, and position with increasing thermal maturation. The related Raman spectroscopic parameters are correlated with the bitumen reflectance in varying patterns and degrees, constrained by the level of maturity.

(2) Among the Raman spectral parameters of the bitumen samples, RBS and $I_D/I_G$ are best maturity indicators, showing a linear correlation with the bitumen reflectance with a correlation coefficient as high as 0.97 within the BRo range of 1.5–3.5% and 3.0–5.0%, respectively.

(3) These two-preferred Raman spectral parameters of the artificial bitumen samples compare well with the natural bitumen samples. With the establishment of a standard method, it is believed that these two parameters could be in practice applied to assessment of maturity of early Paleozoic and Precambrian strata.

## Acknowledgments

The authors are indebted to Dr. Shifeng Dai, Dr. Ron Wilkins, R.W.T. and an anonymous reviewer for their insightful comments and suggestions that have significantly improved the manuscript. This study was jointly supported by the National Key Basic Research Program of China (973 Program, No. 2012CB214705), a Special Funding from the State Major Research Programme of China (No. 2011ZX05008-002-40) and the National Natural Science Foundation of China (No. 41072095). This is contribution No. IS-1764 from GIGCAS.

## References

Beyssac, O., Goffe, B., Chopin, C., Rouzaud, J.N., 2002. Raman spectra of carbonaceous material in metasediments: a new geothermometer. J. Metamorph. Geol. 20, 859–871.
Beyssac, O., Goffe, B., Petitet, J.P., Froigneux, E., Moreau, M., Rouzaud, J.N., 2003. On the characterization of disordered and heterogeneous carbonaceous materials by Raman spectroscopy. Spectrochim. Acta A 59, 2267–2276.
Carolyn, L., Thompson-Rizer, 1987. Some optical characteristics of solid bitumen in visual kerogen preparations. Org. Geochem. 385–392.
Court, R.W., Sephton, M.K., Parnell, J., Gilmour, I., 2007. Raman spectroscopy of irradiated organic matter. Geochim. Cosmochim. Acta 71, 2547–2568.
Dai, S., Jiang, Y., Ward, C.R., Gu, L., Seredin, V.V., Liu, H., Zhou, D., Wang, X., Sun, Y., Zou, J., Ren, D., 2012. Mineralogical and geochemical compositions of the coal in the Guanbanwusu Mine, Inner Mongolia, China: further evidence for the existence of an Al (Ga and REE) ore deposit in the Jungar Coalfield. Int. J. Coal Geol. 98, 10–40.
Ferrari, A.C., Robertson, J., 2000. Interpretation of Raman spectra of disordered and amorphous carbon. Phys. Rev. 61, 14095–14100.
Fu, J.M., Jia, R.F., Liu, D.H., Shi, J.Y., 1989. Organic Geochemistry of Carbonate Rock. Science Press, Beijing (78 pp., in Chinese).
Green, P.D., Johnson, C.A., Thomas, K.M., 1983. Applications of laser Raman microprobe spectroscopy to the characterization of coals and cokes. Fuel 62, 1013–1023.
Guedes, A., Noronha, F., Prieto, C., 2005. Characterisation of dispersed organic matter from lower Palaeozoic metasedimentary rocks by organic petrography, X-ray diffraction and micro-Raman spectroscopy analyses. Int. J. Coal Geol. 62, 237–249.
Guedes, A., Valentim, B., Prieto, A.C., Rodrigues, S., Noronha, F., 2010. Micro-Raman spectroscopy of collotelinite, fusinite and macrinite. Int. J. Coal Geol. 83, 415–422.
Guedes, A., Valentim, B., Prieto, A.C., Noronha, F., 2012. Raman spectroscopy of coal macerals and fluidized bed char morphotypes. Fuel 97, 443–449.
Huang, W.M., Liu, S.G., Xu, G.S., Wang, G.Z., Ma, W.X., Zhang, C.J., Song, G.Y., 2011. Characteristics of paleo oil pools from Sinian to Lower Paleozoic in southeastern margin of Sichuan Basin. Geol. Rev. 57, 285–299 (In Chinese with English abstract).
Jacob, H., 1985. Disperse solid bitumen as an indicator for migration and maturity in prospecting for oil and gas. Erdol Kohle 38, 365–374.
Jacob, H., 1989. Classification, structure, genesis and practical importance of natural solid bitumen (migrabitumen). Int. J. Coal Geol. 11, 65–79.
Jehlicka, J., Urban, O., Pokorny, J., 2003. Raman spectroscopy of carbon and solid bitumens in sedimentary and metamorphic rocks. Spectrochim. Acta A 59, 2341–2352.
Kwiecinska, B., Ruiz, I.S., Paluszkiewicz, C., Rodriques, S., 2010. Raman spectroscopy of selected carbonaceous samples. Int. J. Coal Geol. 84, 206–212.
Kelemen, S.R., Fang, H.L., 2001. Maturity trends in Raman spectra from kerogen and coal. Energy Fuels 15, 653–658.
Kostova, I., Tormo, L., Feo, E.C., Guinea, J.G., 2012. Study of coal and graphite specimens by means of Raman and cathodoluminescence. Spectrochim. Acta A 91, 67–74.
Lin, J.S., Xie, Y., Liu, J.Q., Zhao, Z., Jing, X.Y., Cheng, H., 2011. Restudy of the source rock of Majiang paleo-reservoir. Geol. Sci. Technol. Inf. 30, 105–109 (In Chinese with English abstract).
Liu, D.H., Xiao, X.M., Tian, H., Min, Y.S., Zhou, Q., Cheng, P., Shen, J.G., 2013. Sample maturation calculated using Raman spectroscopic parameters for solid organics: methodology and geological applications. Chin. Sci. Bull. 58, 1285–1298.
Lomando, A.J., 1992. The influence of solid reservoir bitumen on reservoir quality. Am. Assoc. Pet. Geol. Bull. 76, 1137–1152.
Marques, M., Ruiz, S., I., Flores, D., Guedes, A., Rodrigues, S., 2009. Correlation between optical, chemical and micro-structural parameters of high-rank coals and graphite. Int. J. Coal Geol. 77, 377–382.
Muirhead, D.K., Parnell, J., Taylor, C., Bowden, S.A., 2012. A kinetic model for the thermal evolution of sedimentary and meteoritic organic carbon using Raman spectroscopy. J. Anal. Appl. Pyrolysis 96, 153–161.
Quirico, E., Rouzaud, J.N., Bonal, L., Montagnac, G., 2005. Maturation grade of coals as revealed by Raman spectroscopy: progress and problems. Spectrochim. Acta A 61, 2368–2377.
Quirico, E., Montagnac, G., Rouzaud, J.N., Bonal, L., Denise, M., Duber, S., Reynard, B., 2009. Precursor and metamorphic condition effects on Raman spectra of poorly ordered carbonaceous matter in chondrites and coals. Earth Planet. Sci. Lett. 287, 185–193.
Rahl, J.M., Anderson, K.M., Brandon, M.T., Fassoula, C., 2005. Raman spectroscopic carbonaceous material thermometry of low-grade metamorphic rocks: calibration and application to tectonic exhumation in Crete, Greece. Earth Planet. Sci. Lett. 240, 339–354.
Roberts, S., Tricker, P.M., Marshall, J.E.A., 1995. Raman spectroscopy of chitinozoans as a maturation indicator. Org. Geochem. 23, 223–228.
Rogers, M.A., Mcalary, J.D., Balley, N.J.L., 1974. Significance of reservoir bitumens to thermal-maturation studies, western Canada basin. Am. Assoc. Pet. Geol. Bull. 58, 1806–1824.
Schoenherr, J., Littke, R., Urai, J.L., Kukla, P.A., Rawahi, Z., 2007. Polyphase thermal evolution in the Infra-Cambrian Ara Group (South Oman Salt Basin) as deduced by maturity of solid reservoir bitumen. Org. Geochem. 38, 1293–1318.
Schopf, J.W., Kudryavtsev, A.B., Agresti, D.G., Czaja, A.D., Wdowiak, T.J., 2005. Raman imagery: a new approach to assess the geochemical maturity and biogenicity of permineralized Precambrian fossils. Astrobiology 5, 333–371.
Schopf, J.W., Kudryavtsev, A.B., 2009. Confocal laser scanning microscopy and Raman imagery of ancient microscopic fossils. Precambrian Res. 173, 39–49.
Sonibare, O.O., Haeger, T., Foley, S.F., 2010. Structural characterization of Nigerian coals by X-ray diffraction, Raman and FTIR spectroscopy. Energy 35, 5347–5353.
Wopenka, B., Pasteris, J., 1993. Structural characterization of kerogens to granulite-facies graphite: applicability of Raman microprobe spectroscopy. Am. Mineral. 78, 533–577.
Xiao, X.M., Wilkins, R.W.T., Liu, D.H., Liu, Z.F., Fu, J.M., 2000. Investigation of thermal maturity of lower palaeozoic hydrocarbon source rocks by means of vitrinite-like maceral reflectance-a Tarim Basin case study. Org. Geochem. 31, 1041–1052.
Zeng, Y., Wu, C., 2007. Raman and infrared spectroscopic study of kerogen treated at elevated temperatures and pressures. Fuel 86, 1192–1200.
Zhou, Q., Xiao, X.M., Tian, H., Wilkins, R.W.T., 2013. Oil charge history of bitumens of differing maturities in exhumed Palaeozoic reservoir rocks at Tianjingshan, NW Sichuan Basin, southern China. J. Pet. Geol. 36, 363–382.